

Original Research

Use of Satellite Images and the Split Window Algorithm to Detect Fugitive Methane in Tlalnepantla De Baz Landfill

Griselda B. Hernández-Cruz^{1*}, Ann Godelieve Wellens¹, Mario Vásquez-Ortiz², Ruth E. Villanueva-Estrada³, María N. Rojas-Valencia⁴

¹Facultad de Ingeniería, Universidad Nacional Autónoma de México, Ciudad Universitaria, Coyoacán, C.P. 04100, Ciudad de México, México

²Instituto Nacional de Pesca y Acuicultura, SAGARPA, Av. México 190, Del Carmen, Coyoacán, C.P. 04100, Ciudad de México, México

³Instituto de Geofísica, Universidad Nacional Autónoma de México, Ciudad Universitaria, Coyoacán, C.P. 04100, Ciudad de México, México

⁴Instituto de Ingeniería, Universidad Nacional Autónoma de México, Ciudad Universitaria, Coyoacán, C.P. 04100, Ciudad de México, México

Received: 2 March 2022

Accepted: 24 June 2022

Abstract

Worldwide, the increase in land surface temperature has been attributed to the concentration of greenhouse gases. However, there is no record of timely information that shows which types of land cover relate to major increases in surface temperature. The main aim of this paper is to identify the specific sites in a landfill where biogas is released into the atmosphere. A second objective is to try to find a spatial correlation between the concentration of methane emitted to the atmosphere with the observed surface temperature gradients. The recoverable and fugitive methane fluxes were validated with in situ information, using a LICOR gas accumulation chamber. The surface heat estimate was obtained from the Split Window algorithm, using the TIRS sensor of the Landsat 8. With data obtained in previous studies, both in situ and remote, it was possible to spatially correlate the methane flux released into the atmosphere with the temperature distribution plume within the landfill. The importance of our research is related to the continuous need for surface temperature monitoring on the planet. The use of technological tools such as the one presented here reduces the cost and execution time of environmental studies.

Keywords: greenhouse gases, environmental remote sensing, surface temperature estimates, organic waste, wind directions

*e-mail: griselda.hernandez@ingenieria.unam.edu

Introduction

Urban coverage is one of the main soil types to absorb incoming radiation, causing an increase in the environmental temperature. This phenomenon is known as the urban heat island [1]. However, even more important increases in temperature can be attributed to coverage with possible development of greenhouse gases (GHG).

The most common GHG are: carbon dioxide (CO_2), methane (CH_4) and nitrous oxide (N_2O). Besides having a large life period, their concentration has increased significantly in the last decades. CH_4 is the gas that increases the surface temperature the most [2]. Landfills are an important source of atmospheric methane.

Increments in CO_2 and CH_4 concentration have been related directly with vegetation, agriculture and anthropogenic activities [3-5]; however, the contribution of specific sources is unknown as average global concentrations measured in the last decades correspond to aggregate measures, reflecting the contribution of all sources.

Satellite observation techniques and modeling tools are useful for monitoring the Land surface temperature (LST). The advantage of using the above methodologies is that, contrary to the classic methodologies that analyze the surface temperature jointly, they allow to analyze the individual temperature changes observed for different coverages [6, 7].

Another advantage of the use of satellite data is that it allows the LST to be monitored quickly and efficiently over great geographic extensions. Depending on the satellite's trajectory, from some images per month up to several daily images can be obtained. These images can be analyzed with automated techniques, decreasing their analysis time. Conversely, *in situ* sampling requires a considerable investment of time and human capital to obtain, in specific geographical spots and with a digital thermometer, the temperature record [8].

To measure with remote sensors the surface temperature, the thermal infrared portion of the electromagnetic spectrum is needed; if the temperature is due to atmospheric components that emit heat, such as GHG, it is in this portion where the method can detect the energy potential of for example the biogas produced in a landfill [9]. According to Li et al. [10], three methods exist for the recovery of surface temperature with remote techniques: recovery with known emissivity, with unknown emissivity and with unknown atmospheric quantity.

In this paper, we obtain the LST of the Tlalnepantla de Baz landfill with the multi-channel Split-window (SW) algorithm and the amount of biogas emitted to the atmosphere. The aim is to identify a direct relationship between the observed temperature differential and the methane emission in the landfill.

Literature Review

After the launch of satellites that study the earth's surface, worldwide interest has arisen in monitoring the characteristics of the atmosphere. In 1991, the National Aeronautics and Space Administration (NASA) created the Atmospheric Science Data Center (DAAC-ASDC); this center protects the information of around 50 projects and began as a support for the NASA's Earth Observation System (EOS) [11,12].

Among the NASA projects, some satellites missions include the monitoring of atmospheric gases, such as methane; examples are the Measurement of Pollution in the Troposphere (MOPITT), Atmospheric Chemistry (AURA), Interferometric Measurements of Greenhouse Gases (IMG) and The TROPOspheric Monitoring Instrument (TROPOMI) onboard the Sentinel-5 satellites [13]. The corresponding observations are registered at a regional level and study a global worldwide gas emission, without distinguishing the source of methane generation. They cannot be used to determine the presence of emitted gasses locally [14, 15].

At present, the satellites used for the observation of gas concentration have a spatial resolution between 1 and 1000 km^2 , being restricted to the regional monitoring of methane; they cannot be used for local observations, as in the case of landfills where temperature differences resulting from the presence of GHG can be measured or identified with remote sensing techniques [16].

The most precise remote monitoring techniques allowing to quantify biogas in landfills are those that are in direct contact with the site. The sensors are usually mounted on manned aerial platforms; they present results in a short time scale and with a very detailed spatial resolution (centimeters per pixel). However, monitoring costs for these high-precision techniques are high as the required equipment is usually very specialized and requires continuous maintenance. Some samplings also need to be validated with the help of laboratory tests.

Recent advances in terrestrial observations with satellite images allow medium spatial resolutions of 30 m and are able to identify temperature anomalies; in the case of landfills, these anomalies could be correlated with the emitted biogas with the help of *in situ* monitoring.

Our work is in line with that of Buchwitz et al. [17], who obtain a methane fugitive emission measurement and corresponding concentration distribution plume at a landfill in Los Angeles, California. To determine the emission of fugitive methane, they used an *in situ* greenhouse gas analyzer that, in addition to measuring methane, provides meteorological data such as water vapor, types of aerosols present at the site, cloudiness and altitude. To obtain the methane concentration plume, they used an infrared laser spectrometer,

mounted on a manned aerial platform. The flights were programmed to obtain the methane values in an approximate area of 2 km² during 4 continuous days. The results obtained with the spectrometer show a good correlation with in situ measurements and with data observed in NASA's Olinda Alpha Landfill (OAL) program.

Presence of Methane in Landfills

One of the anthropogenic sources that generate GHG are landfills. Due to the use of materials with low permeability in their construction, landfills encapsulate the biodegradable waste and correspondingly the biogas produced by it, mainly methane. The typical biogas composition for these sites is 50-60% CH₄ and 30-40% CO₂. To a lesser extent, hydrogen and sulphide compounds, as well as traces of other gases, can be found [18].

After CH₄ is formed under anaerobic conditions by microbial activity, the mass balance of this gas [18] is:

$$\begin{aligned} \text{CH}_{4 \text{ generated}} &= \text{CH}_{4 \text{ recoverable}} + \text{CH}_{4 \text{ emitted}} \\ &+ \text{CH}_{4 \text{ fugitive}} + \text{CH}_{4 \text{ oxidized}} + \Delta\text{CH}_{4 \text{ stored}} \end{aligned}$$

The elements of the equation are the following:

- CH_{4 recoverable} is the portion of the gas transported by an active system of vertical wells or horizontal collectors (Spokas et al. 2006). Although it is possible to use this portion of the gas as energy, it is not currently done in most Mexican landfills. It is burned because it is less harmful and generates less heat in the form of CO₂ than as methane. CH_{4 recoverable} can be measured by switching off the safety flare.
- CH_{4 emitted} corresponds to the part of methane produced in the landfill and escaping into the atmosphere through the venting wells when the safety flares are not functioning correctly. The emitted

methane is released in the form of gas. In practice, it is difficult to distinguish between CH_{4 emitted} and CH_{4 recoverable}.

- CH_{4 fugitive} represents the methane that is transported sideways at the site. This phenomenon occurs either by lateral hydraulic migration, by contact with non or partially saturated layers, or by a saturation of the superficial fill cover that increases the shallow subsurface pressure. This type of methane is emitted diffusely to the atmosphere. This CH₄ emission varies from 0.0004 to 4000 gm⁻²day⁻¹ and depends on the type of gas recovery installation, conditions and design of the cover and waste type that is disposed of in the site [19].

- CH_{4 oxidized} is oxidized in the landfill cover area where methanotrophic organisms consume methane which, otherwise, could be transported by diffusion to the surface (Popov et al. 2019). A significant portion (10 to 100%) of the CH₄ present in the cover is oxidized, thus preventing its release into the atmosphere [18].

- ΔCH_{4 stored} corresponds to the portion of methane stored and afterwards released in the landfill. This is a temporary process and depends on the amount of methane produced by microorganisms present in the landfill, and therefore difficult to quantify.

Material and Methods

Study Area

The Tlalnepantla de Baz landfill is located on the ancient road to the mines, in the Barrientos area in the municipality of Tlalnepantla de Baz, Estado de Mexico (Fig. 1).

The site has a surface of 44.61 hectares: 28.27 hectares destined to the disposal of solid waste, while the remaining 16.34 hectares correspond to the old dump. The average annual temperature ranges between 12°C and 17°C. The hottest months are May and sometimes

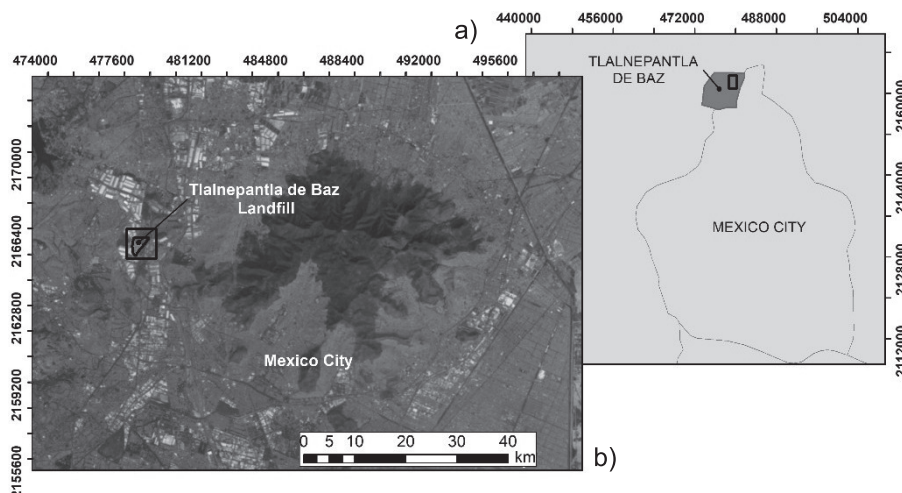


Fig. 1. Study area. a) General view of the location of the landfill. b) Location of the landfill in the north of the municipality.

June, registering an annual average temperature between 16.5°C and 22°C [20].

The waste is disposed of in four cells, which have been built in different stages and have a programmed lifespan of 20 years in total. The cell coating is divided into three layers. The first one is an impermeable layer, mainly composed of the material found at the site. The second layer has a thickness of 30 cm and is composed of clayey material compacted to 90% in its superficial portion. As this porous layer is not the sealing layer, there may be emission of biogas. The most superficial layer is made of construction waste and has an average thickness of 20 cm. Between the latter, water is added to achieve an improved level of compaction. Fig. 2 presents the cell structure in the landfill.

The old landfill, closed in 1998, is located at the northern part of the site. In the southern part, the active cells of the landfill in use can be observed. Cell 1 is the oldest one, created in June 1998. Cell 2 started operating in September 2003 and Cell 3 in May 2008. Cell 4 started receiving waste in September 2013 and is currently the only cell that receives municipal waste.

The residues found in the landfill include organic waste, plastics, glass and slowly decomposing organic material. Hazardous waste, such as batteries, expired medicines, oils and solvents absorbed in materials such as tow and yarn, exists in a lesser proportion.

Manually vented chimneys are installed at the bottom of the cells and grow in height throughout the lifespan of the landfill [20].

Landfill Characterization

The first stage in the present investigation is the characterization of the solid waste arriving

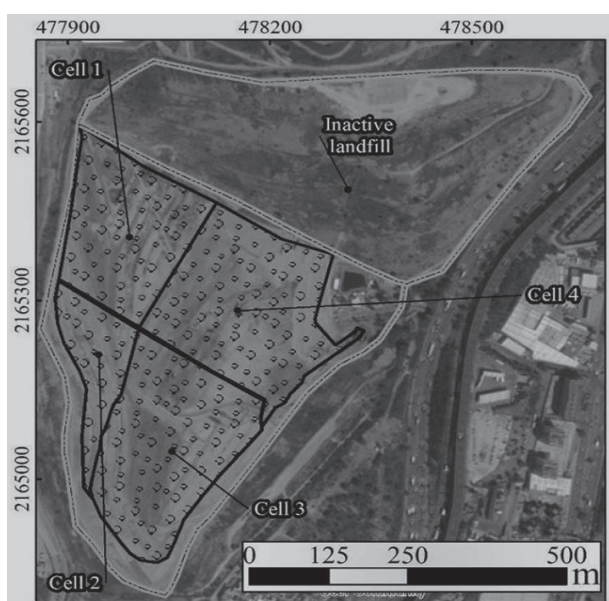


Fig. 2. Location of the four cells of the landfill in use, as well as the old landfill in the northern portion

at the landfill to identify its methane potential, calculate the flow, and identify the cells with the highest methane generation.

The historical volume of waste disposal in the Tlalnepantla landfill was considered. Subsequently, a future projection was generated to estimate how much waste will be disposed of at the end of the landfill's useful life.

Field Work

The second stage in the methodology consisted of validating the theoretical results of the biogas model with measurements. Mønster et al. [21] present an interesting review of available methods to measure fugitive methane emissions from landfills. To detect the presence of diffuse gasses, in this project the West Systems gas accumulation chamber was used. This equipment has a LICOR detector for carbon dioxide (CO₂), a laser detector for methane (CH₄) and an electrochemical cell for hydrogen sulfide (H₂S).

The used equipment passes the gas from the subsoil, which is introduced into the accumulation chamber, to the CO₂, CH₄ and H₂S detectors and then returns them to the accumulation chamber, to record their increase in the chamber. The equipment works with a 1 liter per minute suction pump. A first reading measures the initial gas concentration in the atmospheric air sample from the study site. In a second step, the equipment is placed on the ground surface, trying not to disturb it, in order to determine both the possible existence of a diffuse gas coming from the subsoil, and its accumulation rate.

Application of the Split Window Algorithm

The third stage consisted of temperature recordings in the study site, with remote sensing techniques. The images used to detect LST are Landsat 8 satellite images. The Landsat 8 platform uses a TIRS sensor with electromagnetic information in the region of the thermal infrared spectrum, in two channels: Band 10 corresponding to 10.60-11.19 μm and Band 11, corresponding to 11.50-12.51 μm [22-24].

The images with the sampling data were obtained from the Glovis server [25], which correspond to Path 26 and Row 46. Radiometric corrections were applied to the downloaded images. The brightness temperature was calculated by the Plank inverse.

The images were processed using the Split Window algorithm [25]. The Split Window algorithm estimates the surface temperature based on the graphical information contained in the satellite image. For the verification of the data obtained in the satellite images, in situ temperatures were obtained at 58 sampling points, using Wavetek brand thermometers, model 28XT.

Spatial Analysis of LST and Fugitive Methane Concentrations

In the fourth stage of the work, thematic maps were elaborated using the TerrSet software, developed by Clark Labs. The field data was superposed with the data obtained by means of remote perception techniques, to find a spatial correlation between the LST and the emitted methane concentrations. The fugitive methane emissions were taken on the same day and time that the satellite images were recorded, in order to have the same space and time variables.

The emitted methane is transformed into carbon dioxide, CO₂, through the burning process in the ventilation wells. However, the fugitive methane does not pass the venting well system, and is emitted as CH₄, raising the surface temperature.

Results and Discussion

Split Window Algorithm

Satellite images captured with remote sensing showed consistency with temperatures taken at the landfill with direct instruments. The calibration of the algorithm is done by computational mathematical models, developed in the office.

The use of direct measurement instruments on the study area requires the definition of a grid to take temperatures at specific sites. The mesh data is integrated into a Global Satellite Navigation System, whose data can later be exported to a Geographic Information System to make the thematic map.

The advantages of using algorithms, such as the split window algorithm, is the reduction of time and cost for temperature measurement in landfills, because the work is done from a computer. The algorithm, being calibrated, allows the automation of the methodology, which reduces the possibility of errors in the results. Finally, the validation of the algorithm requires a smaller amount of sampling at the study site.

Landfill Characterization

On average, plastic, disposable diapers and organic residues are the waste that is disposed of in greater proportions in the Tlalnepantla landfill. Conjointly, plastic and disposable diapers generate 34.85% of the disposed waste, while all types of organic waste sum 32.83% (Table 1).

Considering the historical record from the beginning of operations in 2016 and based on the Tlalnepantla waste deposit binnacles, the total volume of waste to date is approximately 250,230 tons. The total disposal volume projected for the landfill is 257,500 tons, considering its age, projected date of closure, typical waste composition and amount of solid waste already disposed of. As about one third of the waste corresponds

Table 1. Waste characterization for the Tlalnepantla landfill.

Subproduct	Average (%)
Waxed cardboard container	0.82
Paperboard	2.87
Aluminum can	0.27
Metal can	0.99
Paper	6.38
Toilet paper	1.86
Disposable diaper	17.48
Bones	0.41
Plastic	17.37
Expanded polystyrene	1.90
Food waste	9.59
Hard vegetal fiber	6.86
Garden waste	4.46
Wood	6.78
Cloth	6.40
Colored glass	4.17
Transparent glass	1.63
Faience and ceramics	0.06
Shoes	2.01
Rubber	0.94
Others	5.90
Fine residue	0.85

to organic compounds, biogas will be generated in the subsoil. Although the landfill was projected to close in 2018, operations were extended, and the site is still functioning as a landfill.

Concentration of Methane in the Biogas

Methane, CH₄, is the main component of biogas. Its emission comes from two sources: the methane that is recovered (and measured) in the venting wells, or recoverable methane, and the methane leaked through the soil, or fugitive methane. The methane measured in the venting wells has maximum values around 76,600 gm⁻² day⁻¹ (Fig. 3a). The fugitive methane measured in the soil was mostly below 0.139 gm⁻² day⁻¹ (Fig. 3b).

The results of the fugitive methane measured on March 28 are classified using the Natural Jenks clustering method, useful for the representation of spatial attributes of data. It is a useful method to analyze geographic variables and it is a good option when the data is unevenly distributed [27, 28]. This method requires few samples for an appropriate representation

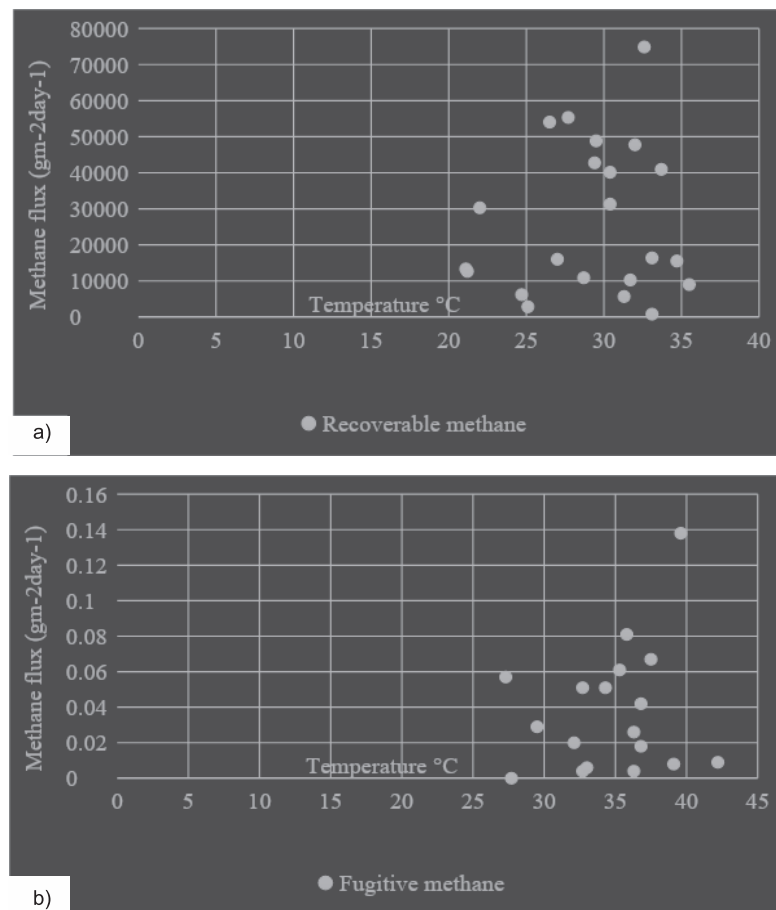


Fig. 3. a) Methane registered in the venting wells, b) Fugitive methane registered in the soil.

and optimizes the classification by reducing the variance within classes and increasing the variance between classes. Its disadvantage is that it is designed for a data set with specific characteristics, so it is not possible to compare maps with different data sets [29].

The venting well methane (CH_4 recoverable) results indicate a greater concentration in cell 3 (Fig. 4), while the methane concentration registered in the soil (CH_4 fugitive) is higher in cell 4 (Fig. 5). As the recoverable methane is burned in the safety flares, and therefore converted to CO_2 , it is not expected to increase the soil temperature. However, due to the magnitude of this methane portion, it is important to quantify it for cases where the flare is not working properly.

Application of the Split Window Algorithm

The satellite images used to obtain the LST correspond to the months of March and August, 2017. In both months, temperatures of around 35°C are found in the landfill coverage. In March, the highest temperatures are recorded in cells 1, 3 and 4 (Fig. 6a). For the month of August, the area of highest temperatures corresponds to cell 4 and, to a lesser extent, cells 1 and 3 (Fig. 6b).

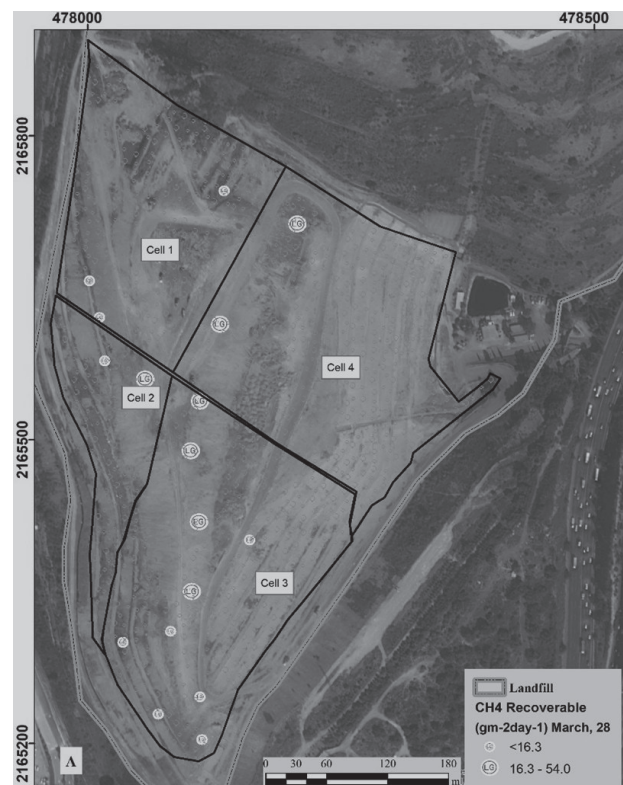


Fig. 4. The interpolated venting well methane distribution plume. Cells 3 and 4 have a higher methane concentration.

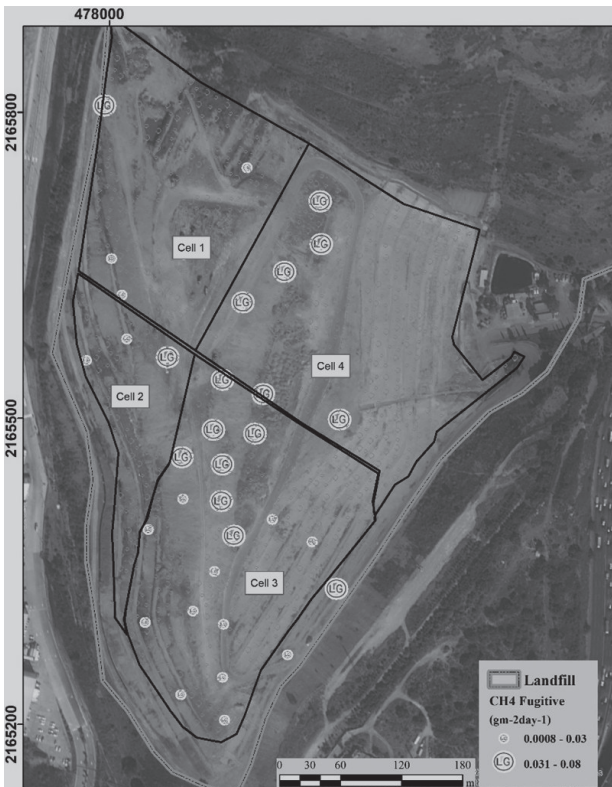


Fig. 5. The interpolated methane fugitive distribution plume. The cell with the largest is cell 4.

Spatial Analysis of LST and Biogas Flux

The spots with the highest methane concentration in the biogas flux fugitive are found in cells 3 and 4. The highest temperatures coincide with cells 3 and 4 as well. The coverage of the sanitary landfill is homogeneous. Since a homogeneous material has the same albedo, the soil temperature in the cells is expected to be homogeneous. However, heterogeneous temperatures were found. Map 7A shows, in grayscale, pixels with temperatures between 30°C to 32.9°C (light gray) up to temperatures of 35.4°C to 37.2°C (dark gray) in all the cells, with the exception of cell 2. In map 7B, in grayscale, there are pixels with temperatures between 25.7°C and 28.2°C (light gray) up to temperatures between 36.9°C and 40.6°C in all cells, except for cell 2.

Since cell 4 is the active cell in the landfill, and due to the fact that the incoming waste is covered with a porous layer, cell 4 is expected to generate the highest flux of fugitive methane in the site. However, it is cell 3 that exhibits the highest fugitive CH₄ flux. As cell 3 has more time without operating than cell 4, there may be a greater activity of the microorganisms that generate GHG. More than 50% of the sample points with high concentrations of fugitive methane were found in cell 3, for both samples (March and August, Fig. 7a) and 7b).

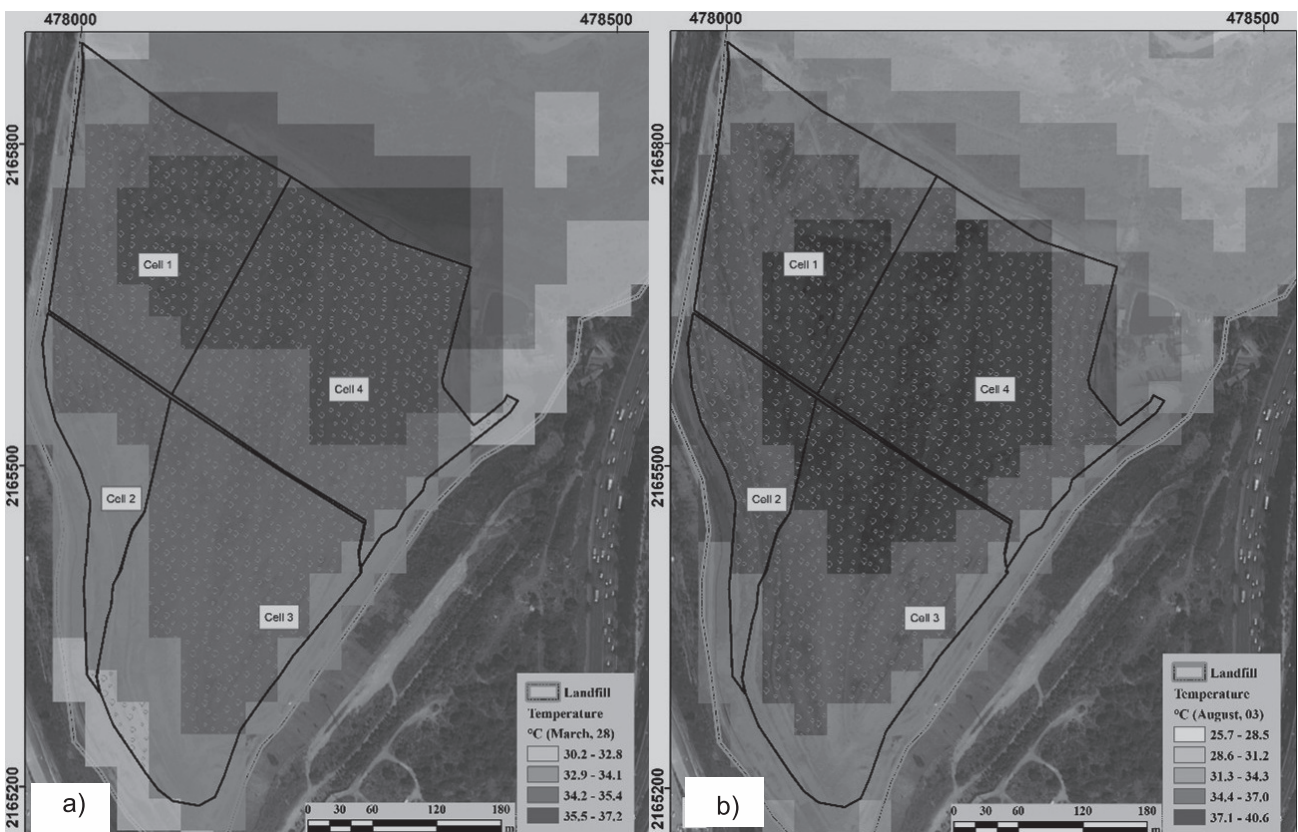


Fig. 6. Landsat 8 Temperature distribution and monitoring sites for fugitive CH₄ in the Tlalnepantla landfill. a) March 2017, b) August 2017.

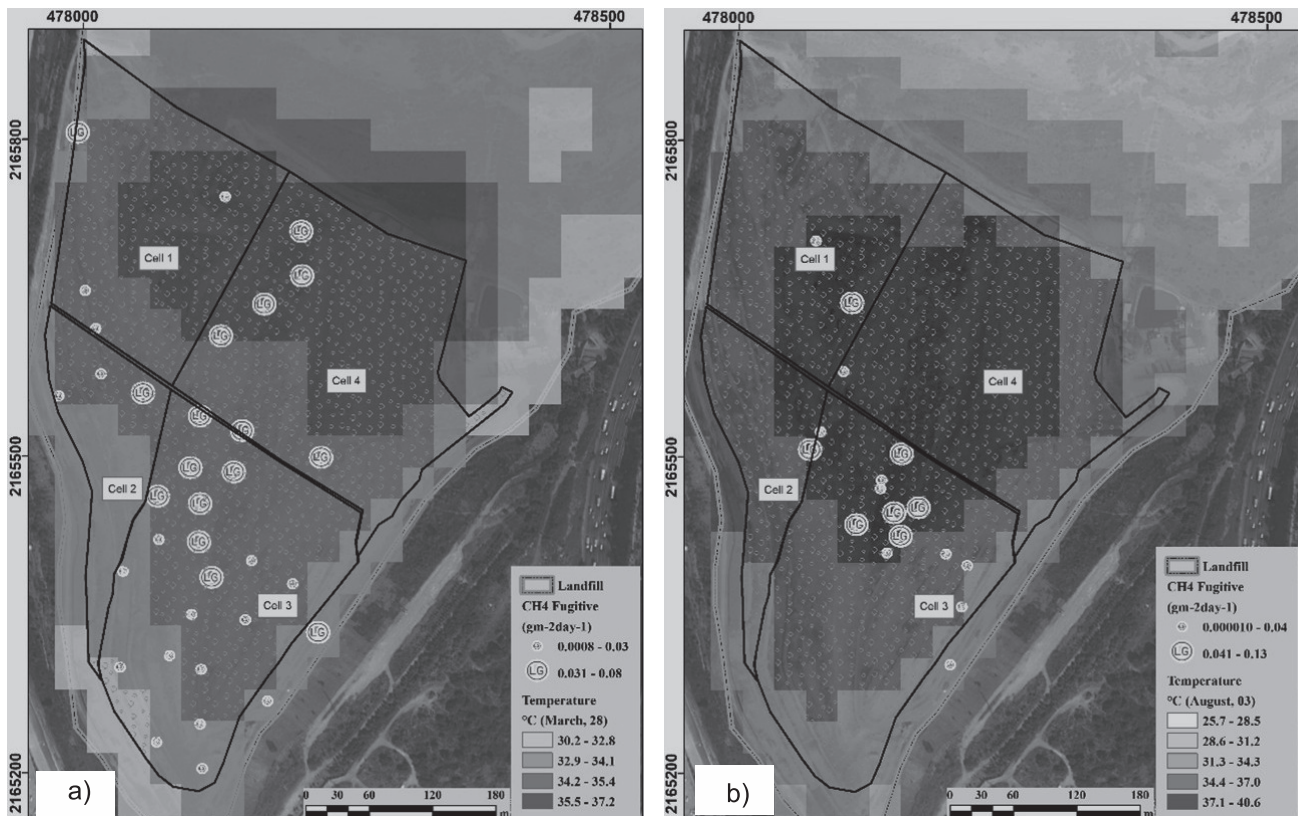


Fig. 7. Landsat 8 Temperature distribution in the Tlalnepantla landfill. a) March 2017, b) August 2017.

Comparing March and August, the fugitive flow increases in August from $0.088 \text{ gm}^{-2} \text{ day}^{-1}$ to $0.138 \text{ g m}^{-2} \text{ day}^{-1}$. The temperature also increased for the month of August, reaching a value of 40.6°C , 3.4°C more compared to the month of March (0.033 to $0.088 \text{ gm}^{-2} \text{ day}^{-1}$ and 37.2°C). According to the results obtained in the study area, the methane emission in the venting wells is three orders of magnitude greater than that of the fugitive CH_4 ; however, it is not released into the atmosphere as it is burned in the pilot burner and converted to CO_2 .

As mentioned before, expected methane emissions are in the order of 0.0004 to $4,000 \text{ gm}^{-2} \text{ day}^{-1}$. The LICOR chamber in some wells registered a supersaturation of gases (until $100,000 \text{ gm}^{-2} \text{ ay}^{-1}$), probably due to the infrastructure of the wells, as they do not have a valve and specific hoses for each type of methane [30] mention a similar problem, since the fluxes measured at the surface were on average $1 \times 10^6 \text{ gm}^{-2} \text{ day}^{-1}$, due concentrations exceeding the detector range (10%).

The measured fugitive CH_4 fluxes oscillate on average between 0.004 and $0.057 \text{ gm}^{-2} \text{ day}^{-1}$. These values are relatively low, so it seems that the soil has a high capacity for methane oxidation. In published literature, values of the order of 0.0002 to $166 \text{ gm}^{-2} \text{ day}^{-1}$ indicate that the landfill is in its final stages of methane generation [31].

Based on experimental results, Lee et al. [32] show that there are significant changes in the CH_4 emission

in landfills, depending on the type of waste. They analyzed the decay rates for four types of common waste (paper, wood, organic and garden waste), finding that they change over time and depend on the amount of degradable organic carbon and, therefore, on the type of waste.

These differences between waste types cause variations in the amount of CH_4 collected. The generation of CH_4 as a result of the decomposition of food waste in tropical climates occurs so rapidly that it leads to significant losses of biogas before the collectors are operational and the register is taken. On the contrary, the decomposition of wood in dry climatic conditions causes delayed emissions, which might be measured after closure of the landfill cell where the residue has been deposited.

The fugitive CH_4 plays an important role in the atmosphere, because it influences the typical air layer temperatures. The main transport mechanism for emitted CH_4 transport from the soil to the atmosphere occurs through diffusion and advection. The CH_4 diffusion disturbs the atmospheric layer, increasing the surface temperature [33].

The month of March, the highest fugitive methane flux values are between 0.033 to $0.088 \text{ gm}^{-2} \text{ day}^{-1}$; the corresponding LICOR temperatures are between 32.1°C and 35.8°C (Fig. 3). For the same ranges of fugitive methane, satellite images show a temperature between 33.5°C and 36.2°C (Fig. 6a). In the month of August, the highest fugitive methane values are in the range

of 0.042 to 0.138 $\text{gm}^{-2} \text{day}^{-1}$, and the LICOR chamber registered temperatures between 36.8°C and 39.6°C (Fig. 3). The pixels in the satellite image that contain fugitive CH_4 values in this range show a temperature between 37.2°C and 39.0°C (Fig. 6b).

The results show that sensors with different characteristics determine similar temperature values. The LICOR chamber is a direct method with an integrated temperature sensor, while the satellite images are processed through an algorithm to obtain the LST.

Kumar et al. [34] developed a regression model for Indian landfills, in which the concentration of CH_4 was correlated to daily temperature fluctuations, to changes in temperature between climatic seasons throughout the year, and to waste mass. Four correlation models were examined, were temperature and waste mass seemed to be the most important factors to predict the CH_4 emission. However, a large amount of variation was not accounted for in this models.

Zhang et al. [35] carried out a study in different regions of China and found that, in the northern hemisphere, there is an increase in CH_4 in summer compared to winter.

Gong and Shi [36] reached comparable results. They performed a monthly analysis of CH_4 in China, showing that summer and autumn have the highest values, while winter and spring have the lowest values. The increase at this time of year is due to environmental factors, such as precipitation, higher temperatures and more hours of sunshine. The emission peak appeared in July, while the lowest value was found in January. The warm conditions of summer, coupled with higher values in the concentration of CH_4 measured in the vents and on the ground, cause an increase in temperature, which is possible to quantify with thermal infrared images.

Nazari et al. [37] wanted to locate thermal anomalies to identify fires within landfills. They applied an algorithm similar to ours, finding consistency between the directly measured temperature and estimation through satellite images from the Landsat 5 and 7 sensor. On average, the temperature variation between the two methods was 6°C.

The use of thermal infrared cameras has indicated indirectly that in locations with GHG generation, the temperature rises to 35-50°C. According to the Wien equation, these temperatures correspond to maximum energy emissivities in a body varying in a spectral range of 8 to 13 μm [38-41].

The TIRS sensor bands cover the spectral range of 10 to 12.5 μm , making it possible to use the Landsat satellite to identify the characteristics of methane.

The LST provides information on temporal and spatial variations of the surface equilibrium and is important for many applications including evapotranspiration, urban climate and the environment [10].

LST determination by remote methods, together with the spatial analysis of the dominant wind speed in

two stations near the landfill allowed observing possible temperature anomalies in the study area.

The LST provides information on temporal and spatial variations of the state of surface equilibrium and is important for many applications including evapotranspiration, urban climate and the environment [10].

The LST, in the monitoring of landfills, allows locating the sites with the greatest potential for methane leakage. The behavior of the temperature distribution associated with spatial variables as the dominant wind direction is one of the variables that can explain the movement of the maximum temperature from the active cell to the inactive ones [42].

Conclusions

The low methane flux measured in soil indicates a good soil capacity for methane oxidation. The high values of the methane flow in the venting wells indicate an important biogas production in all the sampled cells.

The presented methodological proposal seems useful to record the behavior of the methane-temperature system in the landfill. The spatial analysis of the temperature changes recorded in the study area was related to the methane flow being emitted to the atmosphere.

The spatial analysis of the temperature increase was studied with remote sensing techniques and with direct methods (LICOR camera). Concordant temperature ranges were obtained for both methods, being on one hand the estimation by the split window algorithm for satellite images, and on the other the value measured with the integrated sensor for the LICOR camera. Monitoring through satellite images can thus be concluded to be feasible. It implies a lower operation cost and makes the time spent on site validation work more efficient.

In the Tlalnepantla de Baz landfill, biological activity makes it possible to generate biogas even in inactive cells inside the landfill. However, the activity is in the terminal phase. Due to the amount of organic waste, cell four is expected to continue generating biogas; the permeability of the waste confining layers, this biogas will be released into the atmosphere causing an increase in temperature.

The results found in this study for cell 3 of the Tlalnepantla landfill suggests that 40 years after the closure of a landfill cell, a methane generation of up to 160 kg/year can still be observed. The Tlalnepantla landfill was closed in 1998; therefore, according to Lee et al. [32], the generation of biogas for waste with low decomposition rates still continues.

Cell four is the spot in the landfill where an increase of more than 10°C was observed. This increase in temperature was associated with the release of methane into the atmosphere. In order to be able to propose a measure to minimize the adverse effects produced

by the release of methane, it is necessary to obtain a greater amount of data on the methane flow formed in the landfill and determine if it is viable to build specific infrastructure that allows it to be used as an energy source, or to improve the venting wells to convert all recoverable methane to CO₂.

It is important to continue monitoring the study site, in addition to relating the temperature distribution with physical or chemical variables and not only the geographic variable, because the latter may contain biased information. In addition, it is necessary to carry out further studies to establish whether the relationship between the heat distribution boom and the dominant wind direction is correct.

Acknowledgments

This research was partially sponsored through research projects PAPIIT-UNAM program (IA108017).

The authors would like to thank Veolia Mexico group, specially Ing. Jorge Luis Avalos Bueno; CIMMYT, specially Dr. Francelino A. Rodrigues Jr.; IGeo Mexico, specially Dr. Arturo Palencia; eBee and Pix4D, specially Ing. Daniel Soto and Ing. Elías Hernández; Sysmap, specially Ing. Fernando Larios and Ing. Hugo Campuzano for the support for this publication.

Conflict of Interest

The authors declare no conflict of interest.

References

1. STACHE E.E., SCHILPEROORT B.B., OTTELÉ M.M., JONKERS H.H. Comparative analysis in thermal behaviour of common urban building materials and vegetation and consequences for urban heat island effect. *Building and Environment*, 108489, **2021**.
2. AL-GHUSSAIN L. Global warming: review on driving forces and mitigation. *Environmental Progress & Sustainable Energy*, **38** (1), 13, **2019**.
3. CELIK S. The effects of climate change on human behaviors. In *Environment, climate, plant and vegetation growth*. Springer, Cham, 577, **2020**.
4. MIKHAYLOV A., MOISEEV N., ALESHIN K., BURKHARDT T. Global climate change and greenhouse effect. *Entrepreneurship and Sustainability Issues*, **7** (4), 2897, **2020**.
5. TIWARI Y.K., GUHA T., VALSALA V., LOPEZ A.S., CUEVAS C., FERNANDEZ R.P., MAHAJAN A.S. Understanding atmospheric methane sub-seasonal variability over India. *Atmospheric Environment*, **223**, 117206, **2020**.
6. AKTER T., GAZI M., MIA M. Assessment of land cover dynamics, land surface temperature, and heat island growth in northwestern Bangladesh using satellite imagery. *Environmental Processes*, **8** (2), 661, **2021**.
7. KHAMCHIANGTA D., DHAKAL, S. Physical and non-physical factors driving urban heat island: Case of Bangkok Metropolitan Administration, Thailand. *Journal of environmental management*, **248**, 109285, **2019**.
8. SEKERTEKIN A., BONAFONI S. Land surface temperature retrieval from Landsat 5, 7, and 8 over rural areas: Assessment of different retrieval algorithms and emissivity models and toolbox implementation. *Remote Sensing*, **12** (2), 294, **2020**.
9. JACOB F., VIDAL T.H.G, LESAIGNOUX A., OLIOSO A., WEISS M., NERRY F., JACQUEMOUD S., GAMET P., CAILLAULT K., LABARRE L., FRENCH A., SCHMUGGE T., BRIOTTET X., LAGOUARDE J.P. A Simulation-Based Error Budget of the TES Method for the Design of the Spectral Configuration of the Micro-Bolometer-Based MISTIGRI Thermal Infrared Sensor. *IEEE Transactions on Geoscience and Remote Sensing*, **60**, p. 1-19, Art no. 5000919, doi: 10.1109/TGRS.2021.3099896, **2022**.
10. LI Z.L., TANG B.H., WU H., REN H., YAN G., WAN Z., TRIGO I.F., SOBRINO J.A. Satellite-derived land surface temperature: Current status and perspectives. *Remote Sensing of Environment* **131**, 14, **2013**.
11. DE BERNARDI M., PRIANO M.E., FERNÁNDEZ M.E., GYENGE J., JULIARENA M.P. Impact of land use change on soil methane fluxes and diffusivity in Pampean plains, Argentina. *Agriculture, Ecosystems & Environment*, **329**, 107866, **2022**.
12. PLATNICK S. NASA Earth Science Division Operating Missions. Washington, EU: NASA's Earth Observing System. Retrieved from <https://eosps.nasa.gov/content/nasas-earth-observing-system-project-science-office>. **2018**.
13. SCHNEISING, O., BUCHWITZ, M., REUTER, M., BOVENSMANN, H., BURROWS, J.P., BORSODORFF, T., FEUTSCHER, N. M., FEIST, D.G. GRIFFITH, D.W., HASE, F., HERMANS, C., IRACI, L.T., KIVI, R., LANDGRAF, J., MORINO, I., NOTHOLT, J., PETRI, C., POLLARD, D.F., ROCHE, S., SHIOMI K., STRONG, K., SUSSMANN, R., VELAZCO, V.A., WARNEKE, T., WUNCH, D. A scientific algorithm to simultaneously retrieve carbon monoxide and methane from TROPOMI onboard Sentinel-5 Precursor. *Atmospheric Measurement Techniques*, **12** (12), 6771, **2019**.
14. BEER R. TES on Aura mission: Scientific objectives, measurements, and analysis overview. *IEEE Transactions on Geoscience and remote sensing*, **44** (5), 1102, **2006**.
15. JONGARAMRUNGRUANG S., MATHEOU G., THORPE A.K., ZENG Z.-C., FRANKENBERG C. Remote sensing of methane plumes: instrument tradeoff analysis for detecting and quantifying local sources at global scale. *Atmos. Meas. Tech.*, **14**, 7999, **2021**.
16. TURNER A.J., JACOB D.J., BENMERGUI J., BRANDMAN J., WHITE L., RANGLES C.A. Assessing the capability of different satellite observing configurations to resolve the distribution of methane emissions at kilometer scales. *Atmos. Chem. Phys.*, **18**, 8265, **2018**.
17. BUCHWITZ M., SCHNEISING O., REUTER M., HEYMANN J., KRAUTWURST S., BOVENSMANN H., BURROWS J.P., BOESCH H., PARKER R.J., SOMKUTI P., DETMERS R.G., HASEKAMP O.P., ABEN I., BUTZ A., FRANKENBERG C., TURNER A.J. Satellite-derived methane hotspot emission estimate using a fast data-driven method. *Atmospheric Chemistry and Physics* **17** (9), 5751 **2017**.

18. SPOKAS K., BOGNER J., CHANTON J.P., MORCET M., ARAN C., GRAFF C., MOREAU-LE GOLVAN Y., HEBE I. Methane mass balance at three landfill sites: What is the efficiency of capture by gas collection system?. *Waste management*, **26** (5), 516, **2006**.
19. POPOV M., STANKEVICH S., KOSTYUCHENKO Y.V., KOZLOVA A.A. Analysis of Local Climate Variations Using Correlation between Satellite Measurements of Methane Emission and Temperature Trends within Physiographic Regions of Ukraine. *International Journal of Mathematical, Engineering and Management Sciences*, **4** (2), 276, **2019**.
20. SECAM. Caracterización de los residuos que ingresan en el Relleno Sanitario de Tlalnepantla. Reporte técnico, **23**, **2002**.
21. MØNSTER J., KJELDSEN P., SCHEUTZ C. Methodologies for measuring fugitive methane emissions from landfills – A review. *Waste Management*, **87**, 835, **2019**.
22. SAJIB M.Q.U., WANG T. Estimation of Land Surface Temperature in an agricultural region of Bangladesh from Landsat 8: Intercomparison of four algorithms. *Sensors*, **20** (6), 1778, **2020**.
23. PARRILLI S., CICALA L., VINCENZOANGELINO C., AMITRANO D. Illegal Micro-Dumps Monitoring: Pollution Sources and Targets Detection in Satellite Images with the Scattering Transform. In *IEEE International Geoscience and Remote Sensing Symposium, IGARSS*, 4892, **2021**.
24. YANG K., ZHOU X.N., YAN W.A., HANG D.R., STEINMANN P. Landfills in Jiangsu province, China, and potential threats for public health: Leachate appraisal and spatial analysis using geographic information system and remote sensing. *Waste Management*, **28** (12), 2750, **2008**.
25. U.S. Geological Survey. Earth Explorer from: <https://earthexplorer.usgs.gov/>, **2017**.
26. JIMÉNEZ-MUÑOZ J.C., SOBRINO J.A., SKOKOVIĆ D., MATTAR C., CRISTÓBAL J. Land surface temperature retrieval methods from Landsat -8, thermal infrared sensor data. *IEEE Geoscience and Remote Sensing Letters*, **11** (10), 1840, **2014**.
27. ARABAMERI A., SAHA S., ROY J., CHEN W., BLASCHKE T., TIEN BUI D. Landslide susceptibility evaluation and management using different machine learning methods in the Gallicash River Watershed, Iran. *Remote Sensing*, **12** (3), 475, **2020**.
28. BAZ I., GEYMEN A., ER S.N. Development and application of GIS-based analysis/synthesis modeling techniques for urban planning of Istanbul Metropolitan Area. *Advances in Engineering Software*, **40** (2), 128, **2009**.
29. ADLYANSAH A.L., HUSAIN R.L., PACHRI H. Analysis of flood hazard zones using overlay method with figured-based scoring based on geographic information systems: Case study in parepare city South Sulawesi province. In *IOP Conference Series: Earth and Environmental Science*, IOP Publishing, **280** (1), 012003, **2019**.
30. GONZÁLEZ-VALENCIA R., MAGANA-RODRIGUEZ F., CRISTÓBAL J., THALASSO F. Hotspot detection and spatial distribution of methane emission from landfills by surface probe method. *Waste management*, **55**, 299, **2016**.
31. BÖGNER, J.E., SPOKAS, K.A., BURTON, E.A. Kinetics of methane oxidation in a landfill cover soil: temporal variations, a whole-landfill oxidation experiment, and modeling of net CH₄ emissions. *Environ. Science and Technology*, **31**, 2504, **1997**.
32. LEE U., HAN J., WANG M. Evaluation of landfill gas emissions from municipal solid waste landfills for the life-cycle analysis of waste-to-energy pathways. *Journal of Cleaner Production*, **166**, 335, **2017**.
33. YURGANOV L.N., CARROLL D., ZHANG H. Ocean stratification and sea-ice cover in Barents and Kara seas modulate sea-air methane flux: satellite data. *Advances in Polar Science*, 118, **2021**.
34. KUMAR S., NIMCHUK N., KUMAR R., ZIETSMAN J., RAMANI T., SPIEGELMAN C., KENNEY M. Specific model for the estimation of methane emission from municipal solid waste landfills in India. *Bioresource technology*, **216**, 981, **2016**.
35. ZHANG J., HAN G., MAO H., PEI Z., MA X., JIA W., GONG W. The Spatial and Temporal Distribution Patterns of XCH₄ in China: New Observations from TROPOMI. *Atmosphere*, **13** (2), 177. <https://doi.org/10.3390/atmos13020177>, **2022**.
36. GONG S., SHI Y. Evaluation of comprehensive monthly-gridded methane emissions from natural and anthropogenic sources in China. *Science of The Total Environment*, **784**, 147, **2021**.
37. NAZARI R., ALFERGANI H., HAAS F., KARIMI M.E., FAHAD M.G.R., SABRIN S., EVERETT J., OUAYNAYA N., PETERS R.W. Application of satellite remote sensing in monitoring elevated internal temperatures of landfills. *Applied Sciences*, **10** (19), 6801, **2020**.
38. MARTÍN EL., ZHANG J.Y., ESPARZA P., GRACIA F., RASILLA J.L., MASSERON T., BURGASSER A.J. Ammonia-methane ratios from H-band near-infrared spectra of late-T and Y dwarfs. *Astronomy & Astrophysics*, **655**, p-L3, **2021**.
39. GRUNDY W.M., SCHMITT B., QUIRICO E. The Temperature-Dependent Spectrum of Methane Ice O between 0.7 and 5 μm and Opportunities for Near-Infrared Remote Thermometry. *Icarus* **155** (2), 486, **2002**.
40. TANDA G., BALSÌ M., FALLAVOLLITA P., CHIARABINI V. A uav-based thermal-imaging approach for the monitoring of urban landfills. *Inventions*, **5** (4), 55, **2020**.
41. KHALIL M. Record of Atmospheric Methane, In: *Atmospheric Methane: its role in the global environment*, Khalil M., Springer- Verlag Berlin Heidelberg, New York, 1, **2000**.
42. ARONICA S., BONANNO A., PIAZZA V., PIGNATO L., TRAPANI S. Estimation of biogas produced by the landfill of Palermo, applying a Gaussian model. *Waste Management*, **29** (1), 233, **2009**.

